NATIONAL ADVISORY COMMITTEE
FOR AERONAUTICS

TECHNICAL NOTE 3218

FLIGHT DETERMINATION OF THE DRAG AND PRESSURE

RECOVERY OF AN NACA 1-40-250 NOSE INLET

AT MACH NUMBERS FROM 0.9 TO 1.8

By R. I. Sears and C. F. Merlet

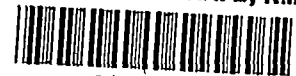Langley Aeronautical Laboratory
Langley Field, Va.

NACA

Washington

July 1955

NATIONAL ADVISORY COMMITTEE FOR AERONAUTICS

TECHNICAL NOTE 3218

FLIGHT DETERMINATION OF THE DRAG AND PRESSURE

RECOVERY OF AN NACA 1-40-250 NOSE INLET

AT MACH NUMBERS FROM 0.9 TO 1.8[1]

By R. I. Sears and C. F. Merlet

SUMMARY

An investigation has been made with rocket-propelled models in free flight to determine the external drag and pressure recovery of the NACA 1-40-250 nose inlet at zero angle of attack. The Mach number range of the tests was from 0.9 to 1.8 and the corresponding Reynolds numbers based on body diameter varied from 4×10^6 to 10×10^6. A technique was developed for varying the internal air flow during flight so that the drag and pressure-recovery characteristics were measured as functions of both mass-flow ratio and Mach number. A pointed parabolic-arc body having the same contour as that of the inlet model aft of the inlet region was also tested to serve as a basis for drag comparison.

The test results indicate that, for mass-flow ratios greater than 0.6 and Mach numbers less than 1.14, the external drag of the inlet model was less than that of the parabolic-body model. At higher Mach numbers the external drag of the inlet model increased rapidly relative to that of the parabolic body. At a Mach number of 1.8 and a mass-flow ratio of 0.9, for example, the external drag of the inlet model was 50 percent greater than that of the parabolic body. The total-pressure recovery at a mass-flow ratio of 0.80 exceeded that for an external-compression supersonic inlet up to a Mach number of about 1.3.

INTRODUCTION

Much data are currently available on the drag of wings and bodies at transonic and supersonic speeds, but data pertaining to the drag associated with air inlets in this speed range are very meager. In order to investigate the transonic characteristics of air inlets, the Pilotless Aircraft Research Division of the Langley Laboratory is undertaking a

---

[1]Supersedes recently declassified NACA RM L50L18, 1951.

series of tests of rocket-propelled models in free flight. The technique involves flying ducted bodies with various types of air inlets and measuring the total drag, the internal drag, and the pressure recovery as functions of Mach number and mass flow.

The NACA 1-40-250 nose inlet was selected to initiate the program. The purpose of testing this inlet, which is of subsonic design, was to determine its transonic and supersonic drag characteristics. In order to help evaluate the extent to which this inlet may be used in the supersonic range without large drag penalties, a somewhat similar, pointed, parabolic-arc body was also tested.

The flight tests give an account of the inlet performance throughout the transonic and well into the supersonic speed range. Because the number of telemeter channels restricts the number of pressure measurements that can be conveniently made, the flight tests are supplemented by ground tests of a more completely instrumented model in the preflight jet at selected Mach numbers. These preflight tests serve as a calibration of the internal flow characteristics of the flight model.

This report presents the results obtained from the tests of the first inlet to be investigated by means of this free-flight technique. All testing was done at the Langley Pilotless Aircraft Research Station at Wallops Island, Va.

SYMBOLS

C_D drag coefficient $\left(\dfrac{D}{\dfrac{\gamma p_o}{2} M_o{}^2 A_f}\right)$

m mass flow through duct

m_o mass flowing through a stream tube of area equal to inlet area under free-stream conditions

V velocity

M Mach number

W weight of model

p static pressure

H total pressure

$\bar{H}$ average total pressure (See appendix)

H_s free-stream pitot stagnation pressure

t   static temperature

D   drag

A   area

γ ratio of specific heats

R   gas constant

y   radial distance from center line of duct at throat station

r   radius of duct at throat station

a   longitudinal-accelerometer reading

g   acceleration due to gravity

Subscripts:

o   free stream

t   throat station

y   radial distance at throat station

x   exit station

f   frontal

i   inlet

I   internal

MODELS, INSTRUMENTATION, AND TESTS

For this investigation, four flight models and one ground-test model were built and tested. Two of the flight models, designated A and B, were without any inlet (fig. 1(a)). The other two flight models, designated C and D, incorporated an NACA 1-40-250 nose inlet forward of the maximum diameter (fig. 1(b)). The ground-test model (fig. 1(c))

had the same nose contour and internal ducting as the inlet flight models.

Basic parabolic-body model.- The basic body used in this inlet investigation had a profile formed by parabolic arcs and is designated herein as the parabolic body. Drawings are shown in figure 2 and coordinates are listed in table I. The fineness ratio was 8.5 and the maximum diameter was located at 42 percent of the body length from the nose. The base diameter was 55 percent of the maximum body diameter. The body was stabilized by four 60° half-delta fins of NACA 65A004 airfoil section. The total exposed fin area was 3.7 square feet. A two-channel telemeter was installed in the parabolic-body models. Longitudinal acceleration and base pressure were measured and telemetered. The base-pressure tube was located in the base cavity near the center line of the model 10.50 inches forward of the aft end of the model.

Inlet model.- Forward of the maximum diameter, the external contour of the ducted flight models was that of the NACA 1-40-250 nose inlet (reference 1). The general arrangement of the model is shown in figure 2 and coordinates are listed in table II. The body shape aft of about one inlet diameter from the nose (fig. 3) and the fins (fig. 2) corresponded almost exactly to those of the basic-body models. The models were built of composite wood and metal construction.

The internal contour of the inlet lips was modified in accordance with the recommendations of reference 2. Some contraction exists at the inlet and a minimum duct area is located just aft of the nose. This minimum section was followed by an 8.2° total-angle conical diffuser having an area ratio of approximately 2:1. At the end of the diffuser, the duct was contracted to form a throat station. Aft of the throat station, four vane-type shutters were installed to govern the mass flow of air. An electric motor caused these shutters to rotate during flight, thereby varying the air flow. For model C, the rate of air-flow variation was about 2.1 cycles per second at M = 1.8 and increased to about 2.7 cycles per second at M = 0.9. For model D, the shutters failed to rotate for most of the supersonic flight, but below M = 0.95 they rotated at about 1.6 cycles per second.

At the throat station, static pressure was measured by six wall orifices equally spaced around the circumference of the duct and manifolded together. At the same station, total pressure was measured by three tubes located at 0, 0.64, and 0.90 radius from the center line of the duct. Base pressure was measured by four inner wall orifices equally spaced circumferentially 1.00 inch from the aft end of the model and manifolded together. Total drag was measured by means of a longitudinal accelerometer. A six-channel telemeter was used to transmit a continuous time history of the five pressure measurements and the accelerometer reading to ground receiving stations.

Flight tests.- For all flight models, velocity was determined from Doppler radar measurements. Ambient air conditions were determined from radiosonde observations. Altitude was computed from the flight path determined by an NACA modified SCR 584 tracking radar. Additional checks on the velocity were obtained from integration of the measured longitudinal acceleration and, in the case of the ducted models, from the total-pressure measurements inside the duct at instants when there was no internal air flow.

All flight models were launched at a 60° angle and accelerated to maximum speed by a Deacon rocket booster (fig. 1). After burnout of the rocket motor, drag separation of the booster from the model occurred. All data were obtained during the ensuing period of coasting flight in which the model decelerated to subsonic speeds.

Preflight-jet tests.- The Langley preflight jet, used for these tests, is located at Wallops Island, Va. The apparatus is of the blowdown, open-jet type and can be fitted with various nozzles for testing at different supersonic and subsonic Mach numbers. Air from two storage spheres is passed through a rotary plug valve and heat exchanger prior to entering the nozzle so that static sea-level atmospheric pressure and temperature can be attained in the jet.

The present tests were made by using the 12-inch Mach number 1.4 nozzle and the 27-inch subsonic nozzle. Although the model was large relative to the 12-inch nozzle, shadowgraph pictures indicate that no disturbances from the nozzle enter the inlet.

The model, shown in figure 1(c), duplicated the nose portion and internal ducting of the flight model. A rake of seven total-pressure tubes and one static-pressure tube, plus six static orifices at the measuring station manifolded together, was used to survey the air flow. Additional measurements along two mutually perpendicular diameters were made at the exit to determine the outgoing momentum.

The mass flow of air was varied by means of four shutters. Tests were made both with the shutters fixed at various positions and with the shutters driven continuously by an electric motor at a very slow speed which also yielded essentially steady-state data. Data were recorded on film as time histories. The model was set at zero angle of attack for all tests.

Test conditions.- The Reynolds number of the flight tests and of the ground tests is shown in figure 4 as a function of Mach number. The values shown are based on the maximum model diameter, 10 inches. Although the ground-test model was the same size as the flight model, the Reynolds numbers of the ground test were somewhat greater than those of the flight tests because sea-level pressure and temperature were maintained in the preflight jet. The angle of attack for all tests was zero.

The method of reduction and analysis of the data is discussed in the appendix. The maximum errors in the absolute magnitude of the data presented are believed to be within the following limits:

C_D . . . . ± 0.01

$\overline{H}/H_O$ . . . . ± 0.01

m/m_O . . . . ± 0.05

M . . . . ± 0.005

The values of C_D and $\overline{H}/H_O$ are most accurate at the higher Mach numbers and the mass-flow ratio is most accurate at large mass flows.

RESULTS AND DISCUSSION

Drag.- The curve of total drag coefficient (including fin and base drag) obtained for the parabolic bodies (models A and B) is presented in figure 5 as a function of Mach number. Also included in this figure are curves of base drag coefficient and estimated fin drag coefficient. The base drag is defined as the product of the base area and the difference between the measured base pressure and free-stream static pressure. The fin drag coefficient has been estimated by assuming a fin drag coefficient of 0.01 based on the exposed fin area. The data obtained indicate that the parabolic body tested has a drag-rise Mach number of 0.98 and reasonably low drag in the supersonic range. The base drag is a small part of the total drag.

The drag-coefficient results for the ducted bodies (models C and D) are presented in figure 6. The curves for the inlet model represent external drag which is defined as the sum of the dragwise components of the gage-pressure and viscous forces acting on the external contour of the model plus the additive drag. In accordance with reference 3, the additive drag is defined as the dragwise component of the gage-pressure forces acting on the entering streamline which divides the external and the internal air flow. The external drag was computed by subtracting from the total drag the internal drag as indicated in the appendix. The solid-line curves present the data obtained with model C. The test points present data obtained with model D. The data presented represent steady-state flow conditions. A discussion of this point is included in the appendix. The curve shown in figure 6 for the parabolic body represents the total drag less the base drag in order to make the data comparable with those shown for the ducted models.

It is apparent from these data that the Mach number for initial drag rise is as high for the NACA 1-40-250 nose-inlet model as for the

parabolic body. At all mass-flow ratios, this drag rise occurs between M = 0.96 and 0.98. At Mach numbers less than about 1.14, the inlet model has less drag than the parabolic body except for mass-flow ratios less than 0.6. Thus, at transonic speeds this inlet has a drag which is as low or lower than that for a good supersonic body.

At higher Mach numbers, however, the drag of the NACA 1-40-250 inlet rapidly becomes much greater than that of the parabolic body even for very large mass-flow ratios. At $M = 1.8$ and $\frac{m}{m_0} = 0.9$, for example, the drag of the inlet model was 50 percent greater than that of the parabolic body. This high drag is attributed to the blunt shape of the inlet in the region forward of a station about one inlet diameter from the nose.

A shadowgraph from the preflight tests at $M = 1.4$, showing the inlet operating at $\frac{m}{m_0} = 0.86$ (fig. 7), shows a strong shock ahead of the inlet. Even if the internal contraction ratio were such as to allow the diffuser to swallow the shock at this Mach number, the blunt inlet shape would not permit an attached shock.

The variation of external drag coefficient with mass-flow ratio is shown in figure 8 for several Mach numbers. The shapes of these curves are quite similar at subsonic and at supersonic speeds. At transonic Mach numbers most of the reduction in drag with mass flow occurs in the range of small mass flows.

The measured variation of C_D with m/m_0 is much less than that of the additive drag alone (reference 3) computed assuming an approximate location of the stagnation point on the lip. The measured external drag, less the computed additive drag, is shown in figure 9 for $M = 1.4$. For reference, the measured drag of the parabolic body, less the base drag, is also shown. These drags represent the component in the drag direction of the viscous and pressure forces acting on the external contour of the body.

It is apparent from this figure that the external pressure drag of the inlet model was less than that of the parabolic body at low mass flows and higher at high mass flows. The pressure-distribution data of reference 4 for a somewhat similar nose inlet (NACA 1-40-200) indicate high suction over the nose at low mass flows and more positive pressures than those computed for the parabolic body at high mass flows. The variations with mass-flow ratio of external pressure drag and of additive drag tend to compensate for each other in a large measure for this particular inlet at all Mach numbers tested. The over-all drag coefficient is high, however, at most supersonic Mach numbers.

Total-pressure recovery.- The ratios of total pressure at the throat station to free-stream pitot stagnation pressure are plotted in figure 10 as functions of $(y/r)^2$ for several values of mass-flow ratio. These data were measured during the preflight-jet tests at $M = 1.4$. The flight-test measurements gave similar distributions throughout the Mach number range. The mass-flow ratio associated with a particular distribution, however, varied somewhat with free-stream Mach number.

The pressure recovery as measured by the ratio of the integrated total pressure at the throat station to the free-stream total pressure is presented in figure 11 as a function of Mach number for several mass-flow ratios. At all supersonic Mach numbers, within the accuracy of the measurements, the measured pressure recovery was equal to that behind a normal shock for $\frac{m}{m_O} = 0$ to 0.4. At $\frac{m}{m_O} = 0.8$, the recovery was about 97 percent of that behind a normal shock at all Mach numbers.

The pressure recovery is plotted as a function of mass-flow ratio for several Mach numbers in figure 12. The results from the preflight-jet tests are also shown as dashed curves for $M = 0.9$ and 1.4. The agreement of the ground-test and flight-test measurements is good.

The pressure recoveries of the present tests are compared in figures 11 and 13 with those reported in reference 3 for an external-compression supersonic inlet (Ferri type, $30°$ cone). It is apparent from figure 11 that, at mass-flow ratios below 0.8, the recovery of the subsonic-diffuser model is excellent below a flight Mach number of 1.3. On the other hand, it is apparent from the same figure that, at a mass-flow ratio of 0.8, the pressure recovery of the supersonic diffuser is higher than that of the subsonic diffuser above a Mach number of approximately 1.3. It may also be noted in both figures 11 and 13 that a mass-flow ratio of 0.9 was the highest obtained by the subsonic diffuser and the recovery was poor, whereas the supersonic diffuser had relatively good recovery at mass-flow ratios as high as 1.0. Apparently, partial choking of the inlet and separation in the diffuser occurred at the high mass-flow ratios for the subsonic diffuser. Even in the subsonic flight range from $M = 0.9$ to $M = 1.0$ the pressure recovery decreased markedly at mass-flow ratios greater than 0.8 (fig. 12). These characteristics are probably typical of any open-nose inlets with similar internal geometry.

CONCLUSIONS

Free-flight tests of the NACA 1-40-250 nose inlet and of a similar, pointed parabolic-arc body at zero angle of attack have indicated the following:

1. Initial drag rise for the inlet model at all mass-flow ratios and for the parabolic body started at Mach numbers of about 0.96 to 0.98.

2. For Mach numbers less than 1.14 and mass-flow ratios greater than 0.6, the external drag of the inlet model was less than that of the parabolic body.

3. As the Mach number increased beyond 1.14, the external drag of the inlet model deviated rapidly from and soon became excessive relative to that of the parabolic body, even for large mass-flow ratios. At a Mach number of 1.8 and a mass-flow ratio of 0.9, for example, the drag of the inlet model was 50 percent greater than that of the parabolic-body model.

4. At a mass-flow ratio of 0.80, the total-pressure recovery of this nose inlet and diffuser combination exceeded that of an external-compression supersonic inlet at Mach numbers less than about 1.3, whereas the reverse is true at higher Mach numbers.

Langley Aeronautical Laboratory,
    National Advisory Committee for Aeronautics,
        Langley Field, Va., December 19, 1950.

APPENDIX

METHOD OF ANALYSIS

The four pressure measurements at the throat station served to determine the mass flow and the total-pressure distribution at the end of the diffuser. Ground tests indicated that the flow at this station was reasonably symmetrical about the duct center line. For the flight model, the velocity distribution measured on one radius was therefore assumed to be valid for all radii. The average total pressure and the mass flow were determined by integration of the measured profiles as indicated by the following expressions:

$$\bar{H} = \int_0^1 H \, d\left(\frac{y}{r}\right)^2$$

$$m = \left[\frac{\gamma}{gRt_0\left(1 + \frac{\gamma - 1}{2}M_0^2\right)}\right]^{1/2} A_t p_t \int_0^1 M_t \sqrt{1 + \frac{\gamma - 1}{2}M_t^2} \, d\left(\frac{y}{r}\right)^2$$

Free-stream total pressure and pitot stagnation pressure were computed from the velocity measured by the Doppler radar and the ambient air conditions measured by the radiosonde. The calculated pitot stagnation pressure agreed within ±2 percent with the four pressure measurements at the throat when the internal mass flow was zero.

The mass which would flow through an area equivalent to the inlet area under free-stream conditions was determined as follows:

$$m_0 = \left(\frac{\gamma}{gRt_0}\right)^{1/2} p_0 M_0 A_i$$

The internal force (drag in this case) was defined in a manner consistent with current practice for turbojet engines. Thus,

$$D_I = m\left(V_0 - V_x\right) - \left(p_x - p_0\right)A_x$$

This equation defines the internal drag as the dragwise component of the gage-pressure and viscous forces acting on the inside surfaces of the model minus the additive drag (reference 4). All quantities in this expression were directly measured except the exit velocity. An average exit velocity was computed from the known mass flow, exit static pressure, and exit area, by using one-dimensional compressible-flow theory. Ground tests showed that the measured momentum at the exit agreed within 1 percent with the exit momentum computed in the manner just indicated.

The external drag of the flight models was evaluated as follows:

$$D = W\frac{a}{g} - D_I$$

Because of the relatively fast pulsing rate used, the mass of air within the duct underwent large accelerations (of the order of 300g for model C). When the shutters were wide open or closed, they effectively maintained this condition long enough relative to the resonant period of the flow in the duct so that the quantities measured and computed by the above equations are truly representative of steady-state conditions. The quantities computed while the flow-regulating shutters are opening or closing, however, are not steady-state values but are affected by the time rate of change of velocity of the air within the duct. In order to reduce the effects of these accelerations to values much less than the other experimental errors, the drag, mass flow, and pressure recovery were plotted as a function of Mach number for various constant positions of the duct shutters. The steady-state value of the quantity at a given Mach number and shutter position was taken as the average of its value when the shutters were opening and of its value when the shutters were closing.

For model C, the maximum deviation from the mean of any of the values measured with accelerating or decelerating flow amounted to $\Delta C_D = \pm 0.02$ and $\frac{\Delta H}{H_o} = \pm 0.01$. The drag and total pressure were greater than their respective steady-state values when the flow was decelerating and less when it was accelerating. Because the errors due to accelerating and decelerating flow are certainly of opposite sign and because the deviation from the mean is of the same order of magnitude as the other experimental errors, it is believed that the averaging process used reduces the transient errors to entirely acceptable values.

For model D, during the portion of the flight in which the Mach number decreased from 1.8 to 1.16, the shutters did not turn but remained in the closed position. Steady-state values for zero mass flow were therefore obtained over this range of Mach numbers. From Mach number 1.16 to

about 1.05, the shutters turned slowly through one-quarter revolution
to the wide-open position. Over this range of Mach numbers, the time
rate of change of mass flow was only one-fifth that of model C. From
Mach number 1.05 to about 0.95, the shutter remained in the wide-open
position and steady-state values for maximum mass flow were obtained
in this transonic range. At Mach numbers less than 0.95, the shutters
rotated continuously at a pulsing rate of 1.6 pressure-cycles per second.

The cause of this rather erratic behavior of the pulsing gear in
model D is attributed to the fact that the driving motor was purposely
made to operate on half-rated voltage in order to slow the pulsing
rate. However, the data obtained under actual steady-state conditions
and during the one very slow pulse between M = 1.16 and 1.05 afforded
the opportunity to check the validity of the procedure used to reduce
the data of model C to steady-state conditions.

It can be seen in figure 6 that the drag data for models C and D
are in excellent agreement. It is therefore indicated that the transient
components in the measured quantities of model C have been reduced to
negligible values.

REFERENCES

1. Baals, Donald D., Smith, Norman F., and Wright, John B.: The Development and Application of High-Critical-Speed Nose Inlets. NACA Rep. 920, 1948. (Supersedes NACA ACR L5F30a.)

2. Nichols, Mark R., and Keith, Arvid L., Jr.: Investigation of a Systematic Group of NACA 1-Series Cowlings With and Without Spinners. NACA Rep. 950, 1949. (Supersedes NACA RM L8A15.)

3. Ferri, Antonio, and Nucci, Louis M.: Preliminary Investigation of a New Type of Supersonic Inlet. NACA Rep. 1104, 1952. (Supersedes NACA TN 2286.)

4. Pendley, Robert E., and Robinson, Harold L.: An Investigation of Several NACA 1-Series Nose Inlets With and Without Protruding Central Bodies at High-Subsonic Mach Numbers and at a Mach Number of 1.2. NACA TN 3436, 1955. (Supersedes NACA RM L9L23a.)

TABLE I - COORDINATES FOR PARABOLIC BODY

[All dimensions are in inches]

Station	Radius
0	0
4.00	1.06
8.00	2.00
12.00	2.80
16.00	3.48
20.00	4.06
24.00	4.47
28.00	4.76
32.00	4.95
36.00	5.00
40.00	4.99
44.00	4.93
48.00	4.85
52.00	4.74
56.00	4.59
60.00	4.42
64.00	4.21
68.00	3.97
72.00	3.70
76.00	3.41
80.00	3.07
83.50	2.75
85.00	2.75

NACA

TABLE II - COORDINATES FOR NACA 1-40-250 INLET BODY

[All dimensions are in inches]

Station	Radius
12.00	2.07
12.05	2.21
12.15	2.31
12.25	2.38
12.50	2.50
12.75	2.61
13.00	2.70
14.00	3.00
15.00	3.25
16.00	3.45
20.00	4.04
24.00	4.45
28.00	4.74
32.00	4.92
36.00	5.00
40.00	4.99
44.00	4.93
48.00	4.85
52.00	4.74
56.00	4.59
60.00	4.42
64.00	4.21
68.00	3.97
72.00	3.70
76.00	3.41
80.00	3.07
83.50	2.75
85.00	2.75
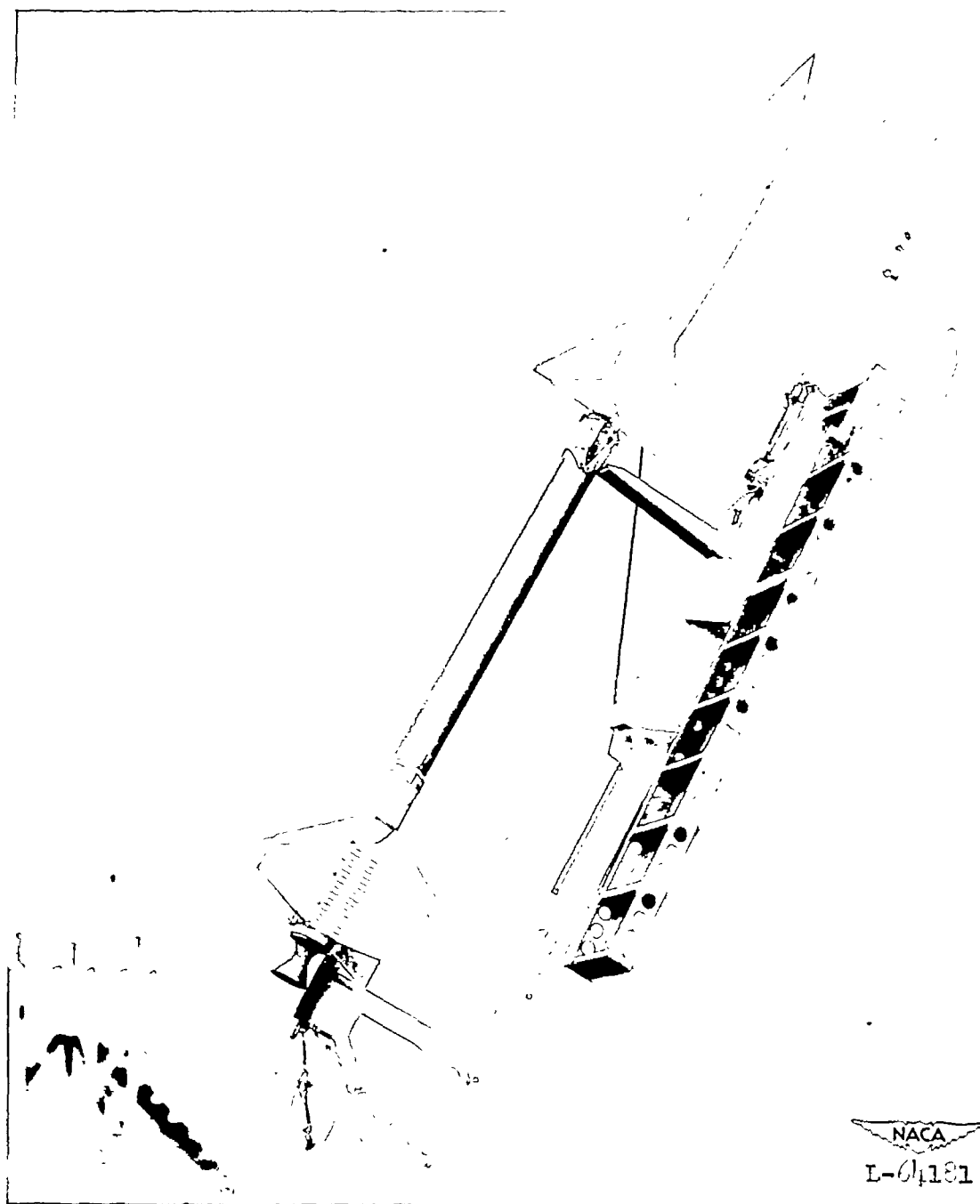
(a) Parabolic-body model on the launcher.

Figure 1.- Photographs of the models.
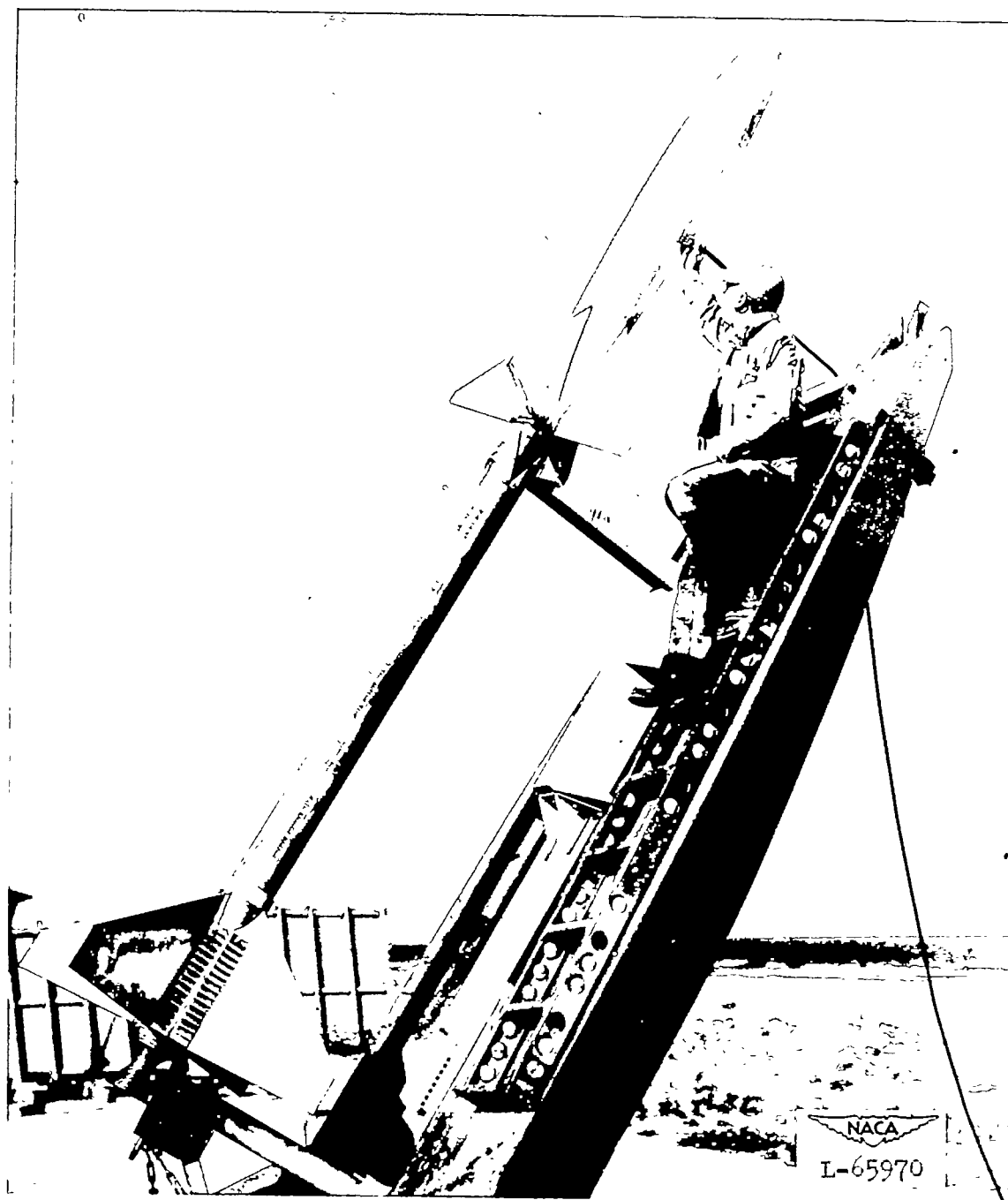
(b) NACA 1-40-250 inlet model on the launcher.

Figure 1.- Continued.
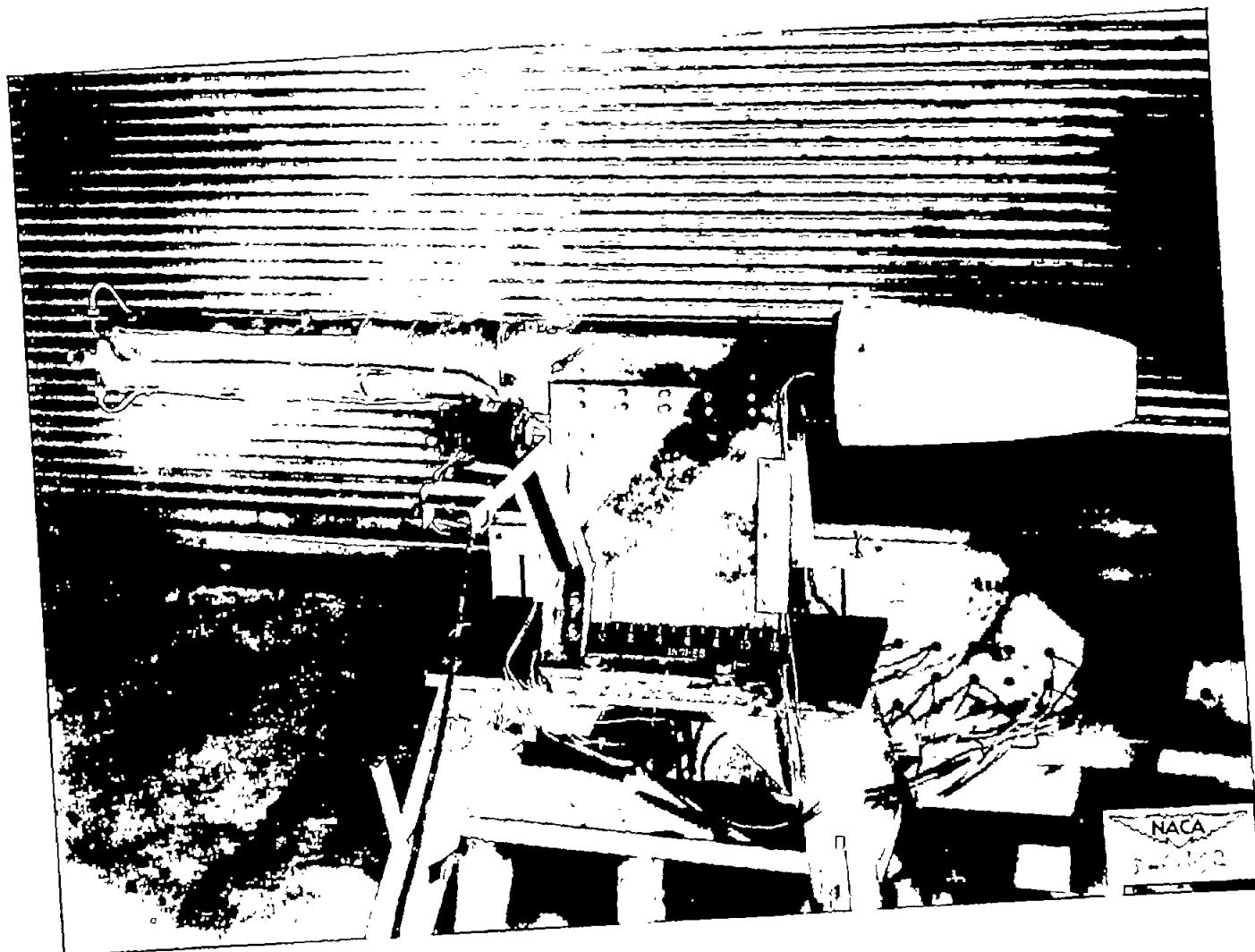
(c) Ground-test model in the preflight jet.

Figure 1.- Concluded.
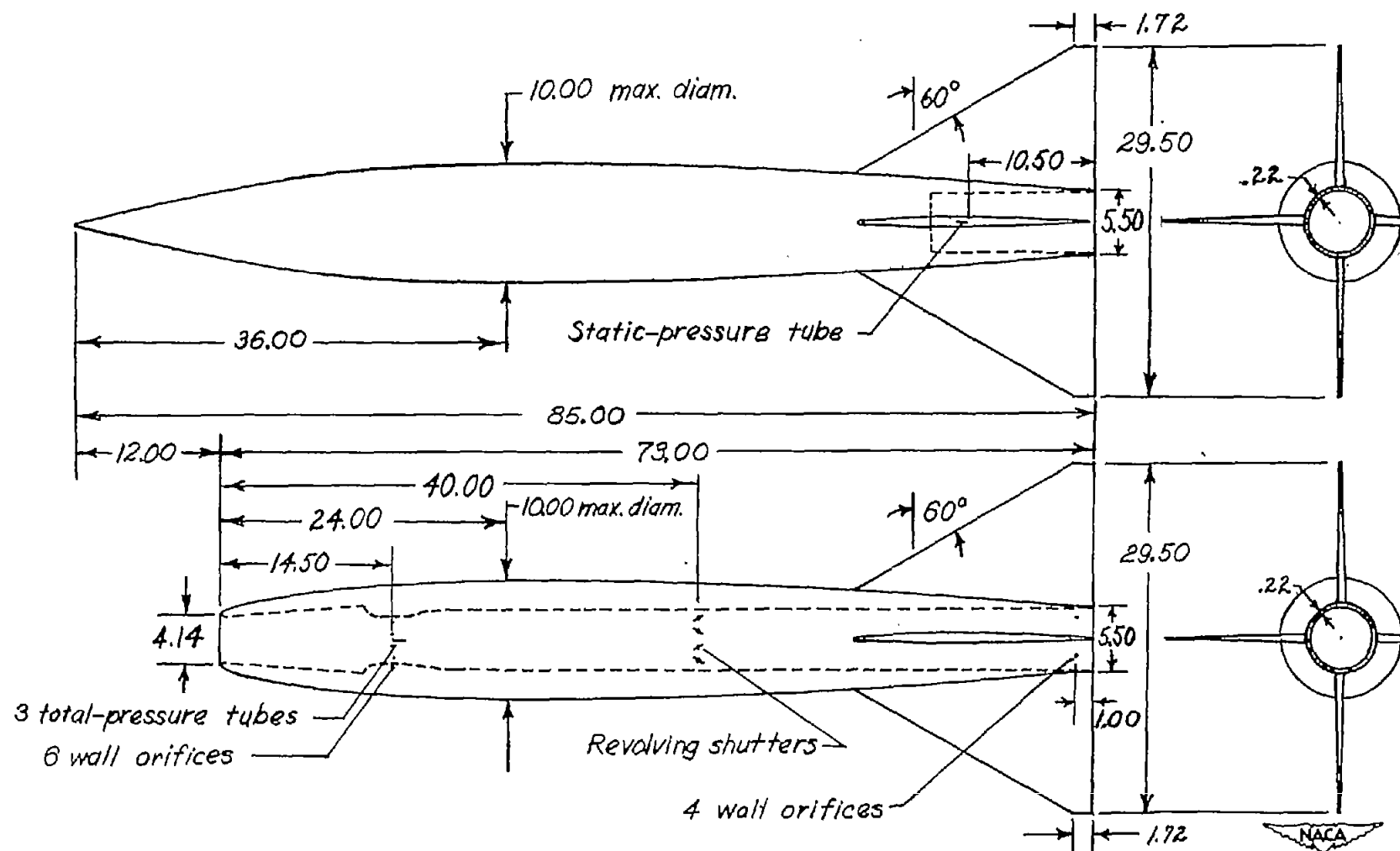
Figure 2.- General arrangement of flight models. (All dimensions are in inches.)

x	r
0	2.07
0.07	1.99
.25	1.94
.44	1.93
.59	1.93

Constant diam. duct

3.85 min. diam.

.52

8.2°

5.96

4.00

4.14

x

r

Contour of parabolic body

12.00

14.50
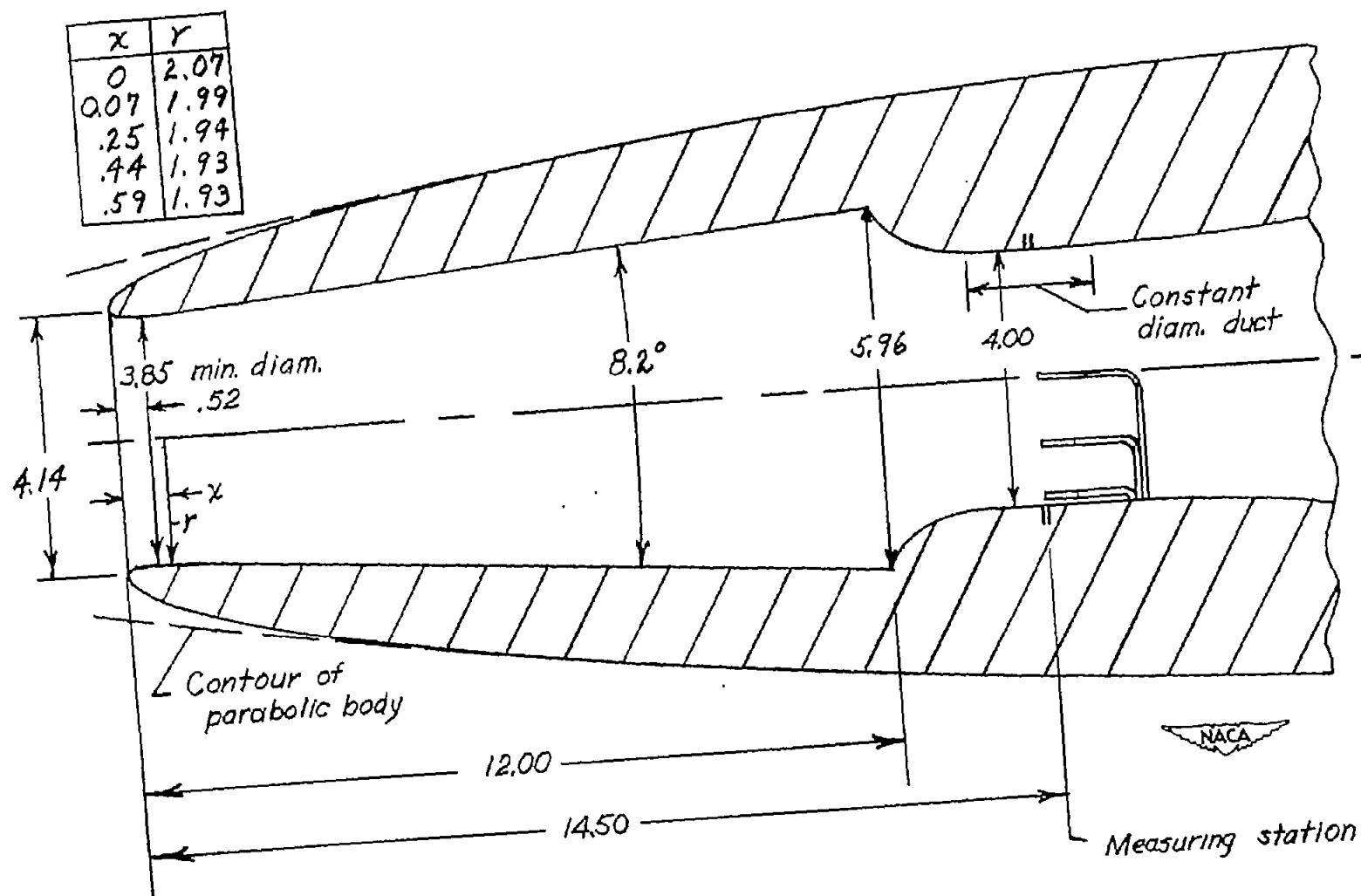
Measuring station

Figure 3.- Details of inlet, diffuser, and measuring sections. (All dimensions are in inches.)
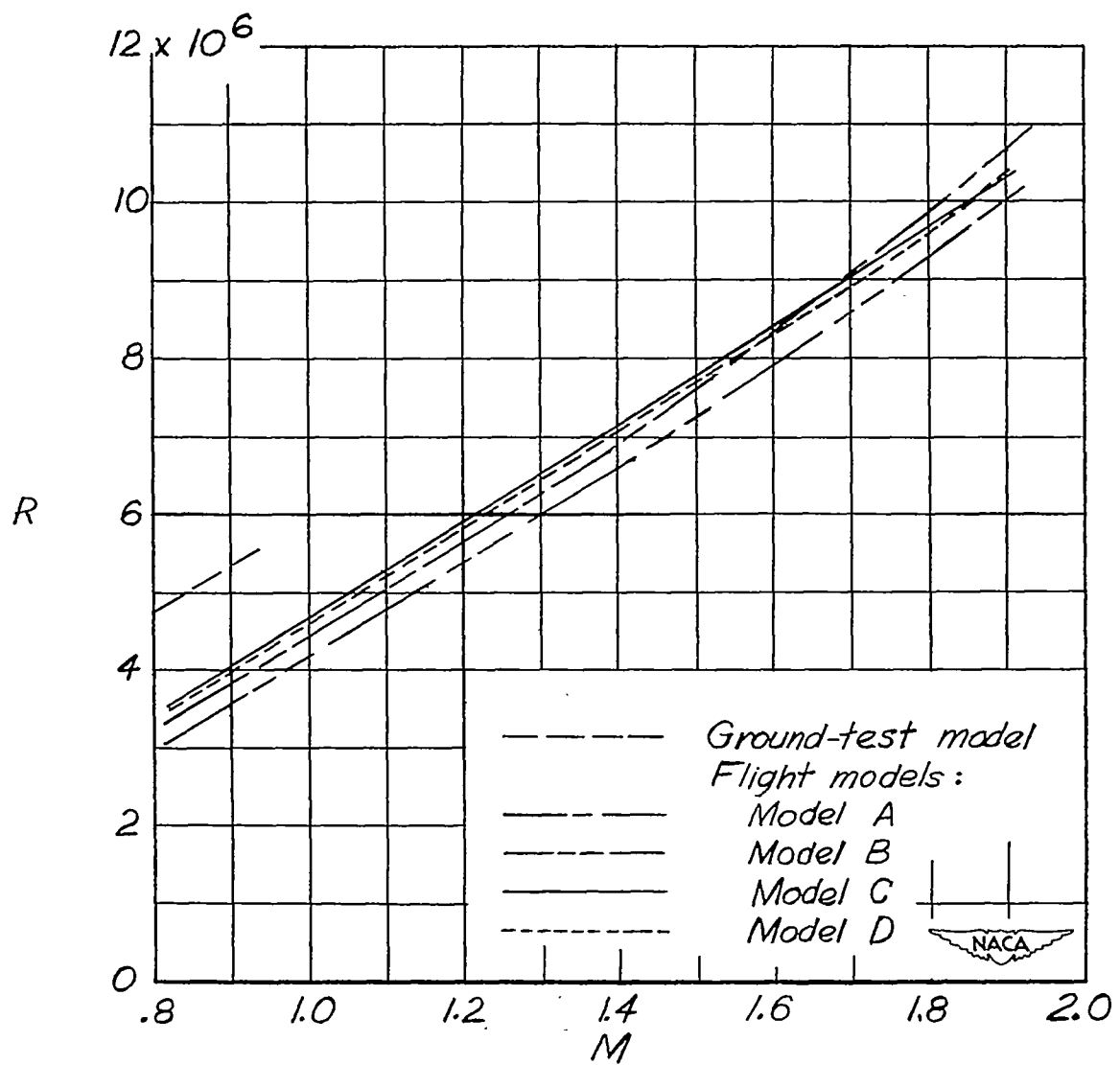
Figure 4.- Variation of Reynolds number R with Mach number M. Reynolds numbers are based on maximum body diameter of 10 inches.
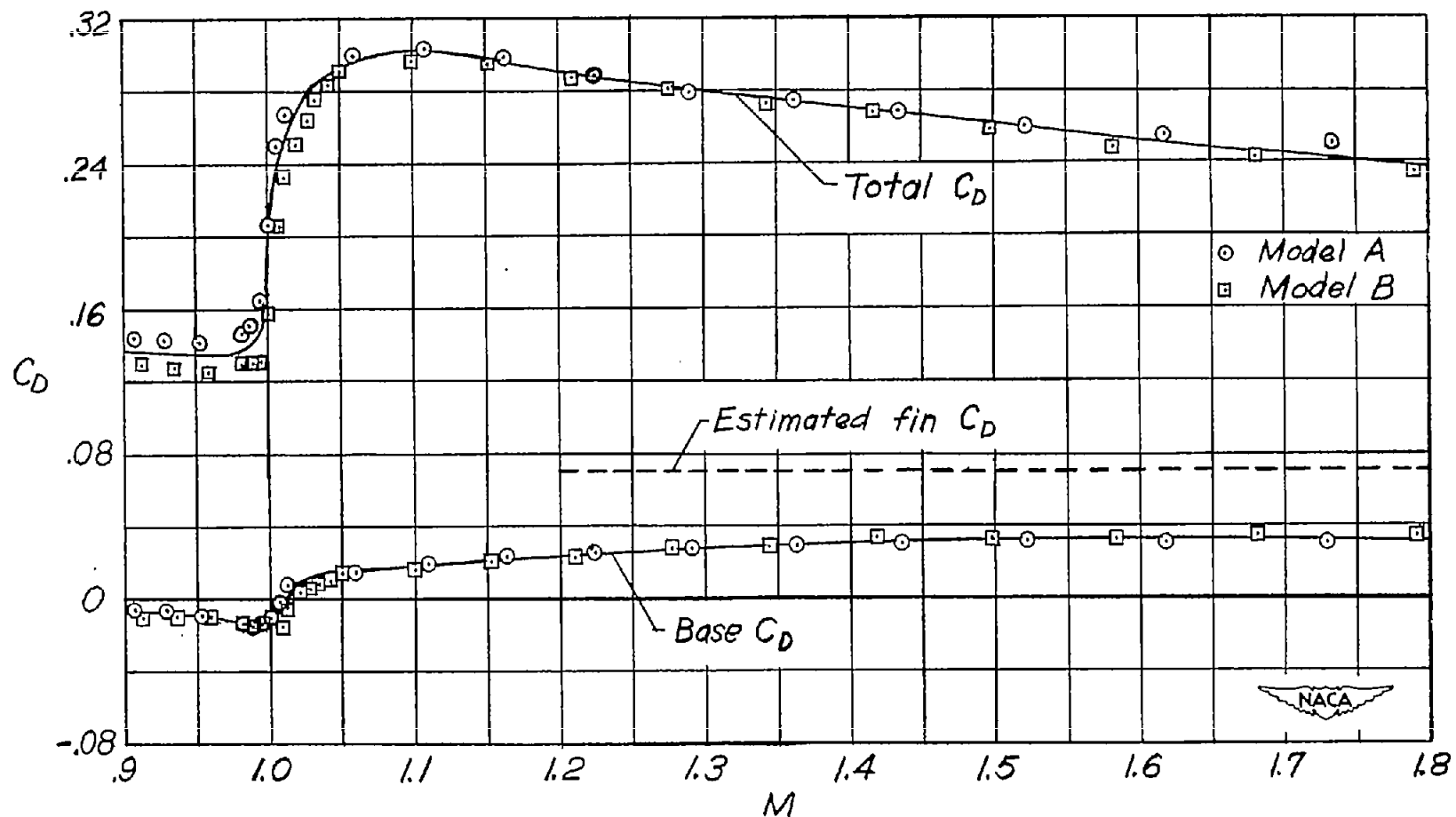
Figure 5.- Total and base drag coefficients as a function of Mach number for parabolic body.
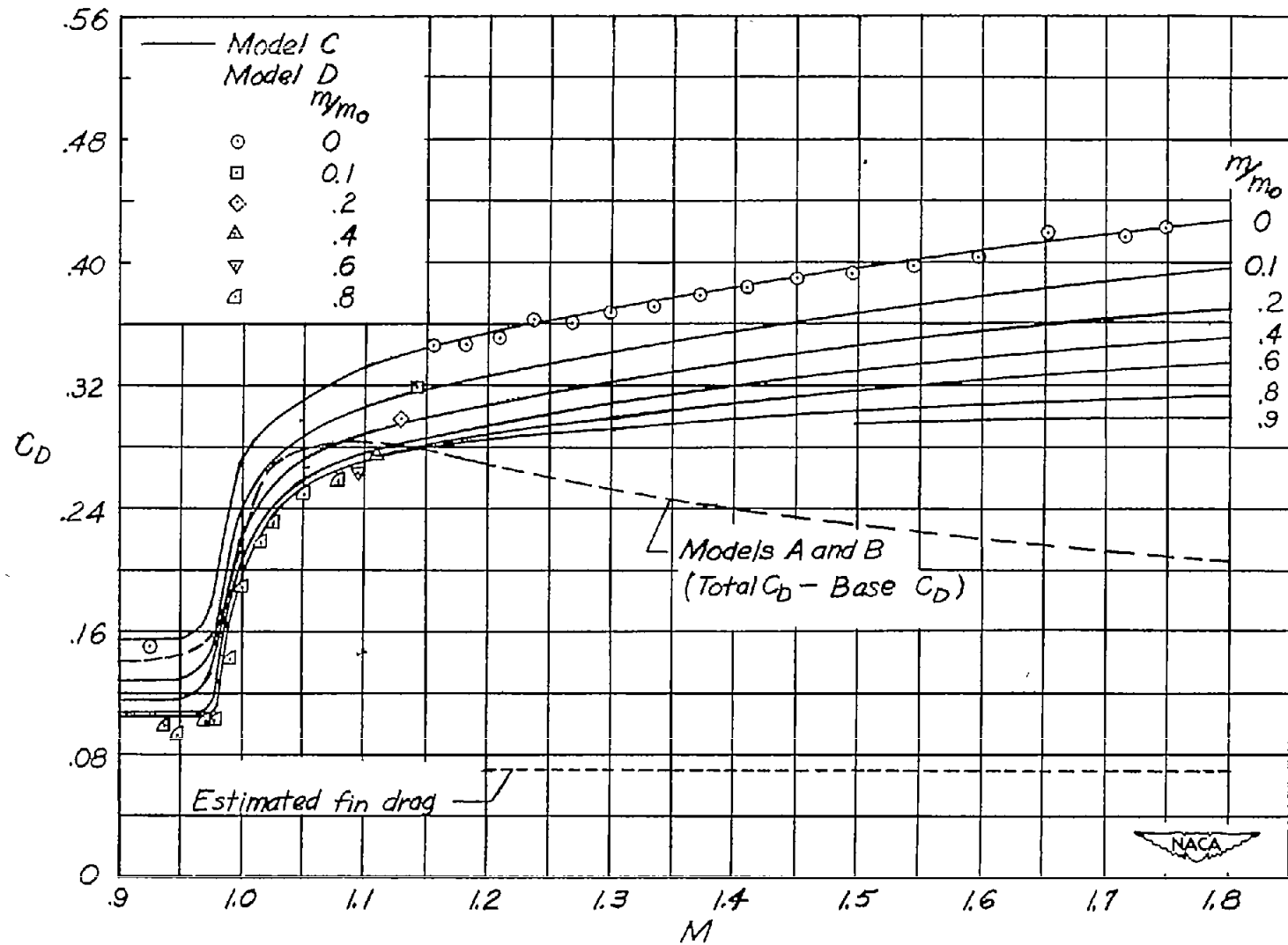
Figure 6.- Variation of external drag coefficient with Mach number for several mass-flow ratios.
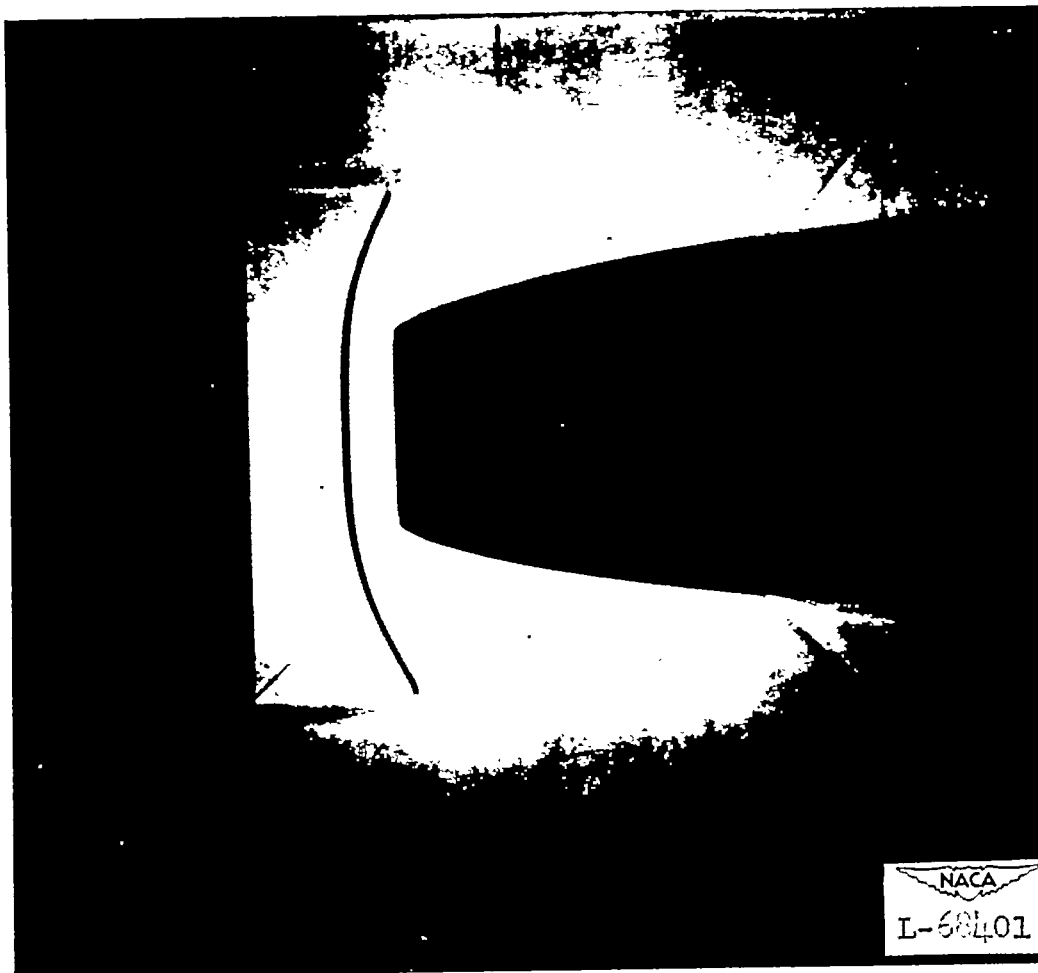
Figure 7.- Shadowgraph of NACA 1-40-250 nose-inlet model in preflight

jet. M = 1.4; $\frac{m}{m_0}$ = 0.86.
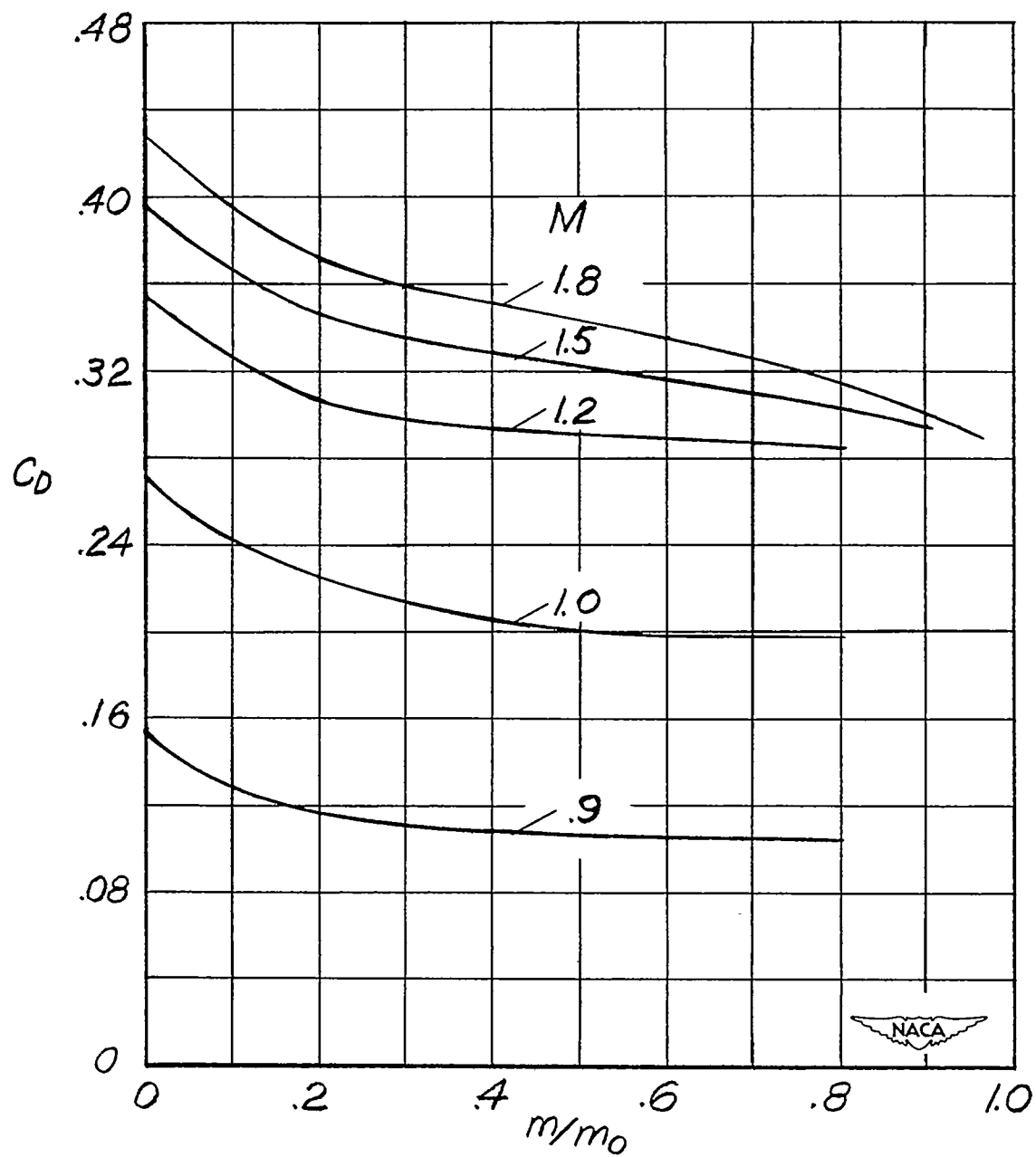
Figure 8.- Variation of external drag coefficient with mass-flow ratio at several Mach numbers.
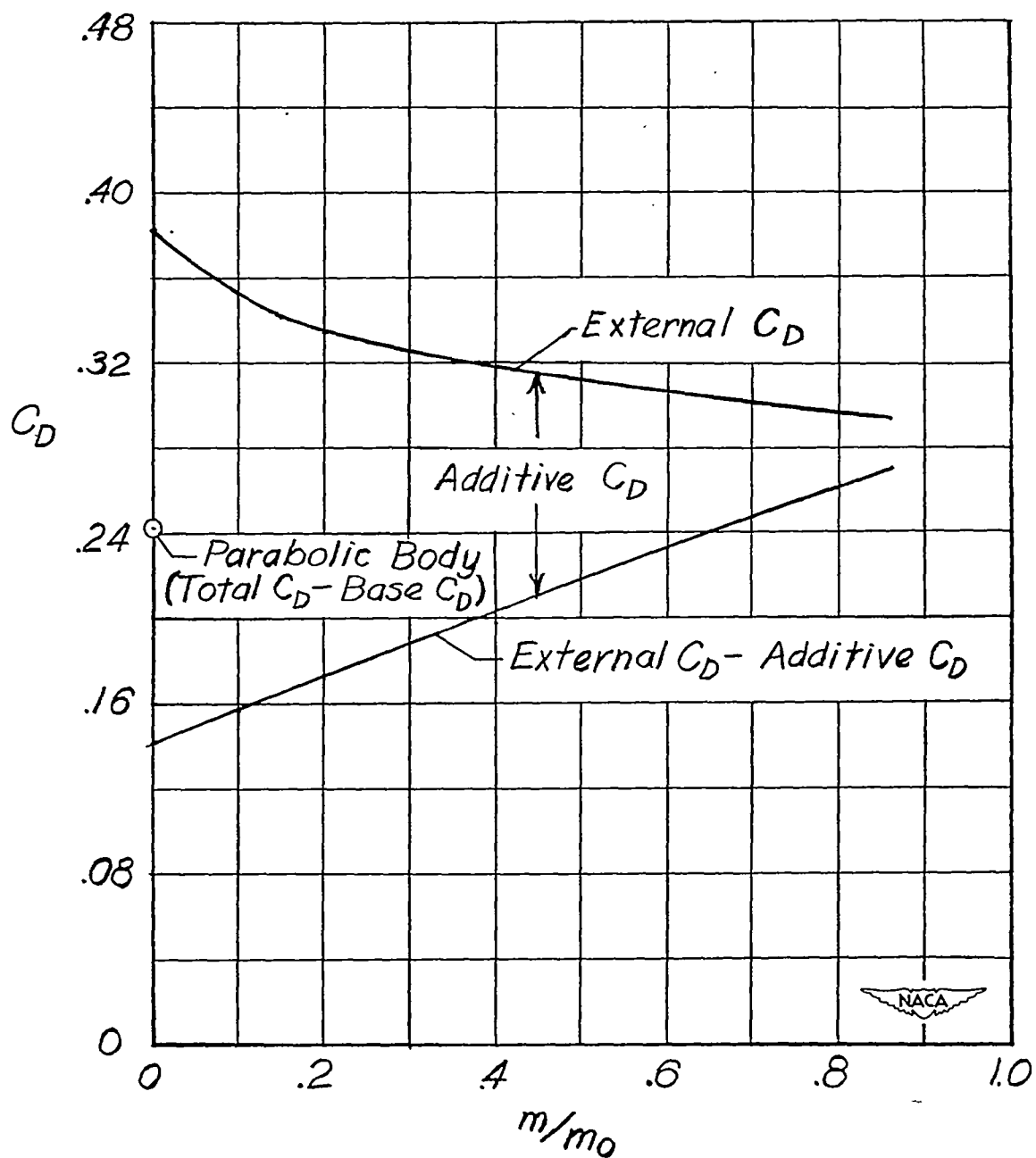
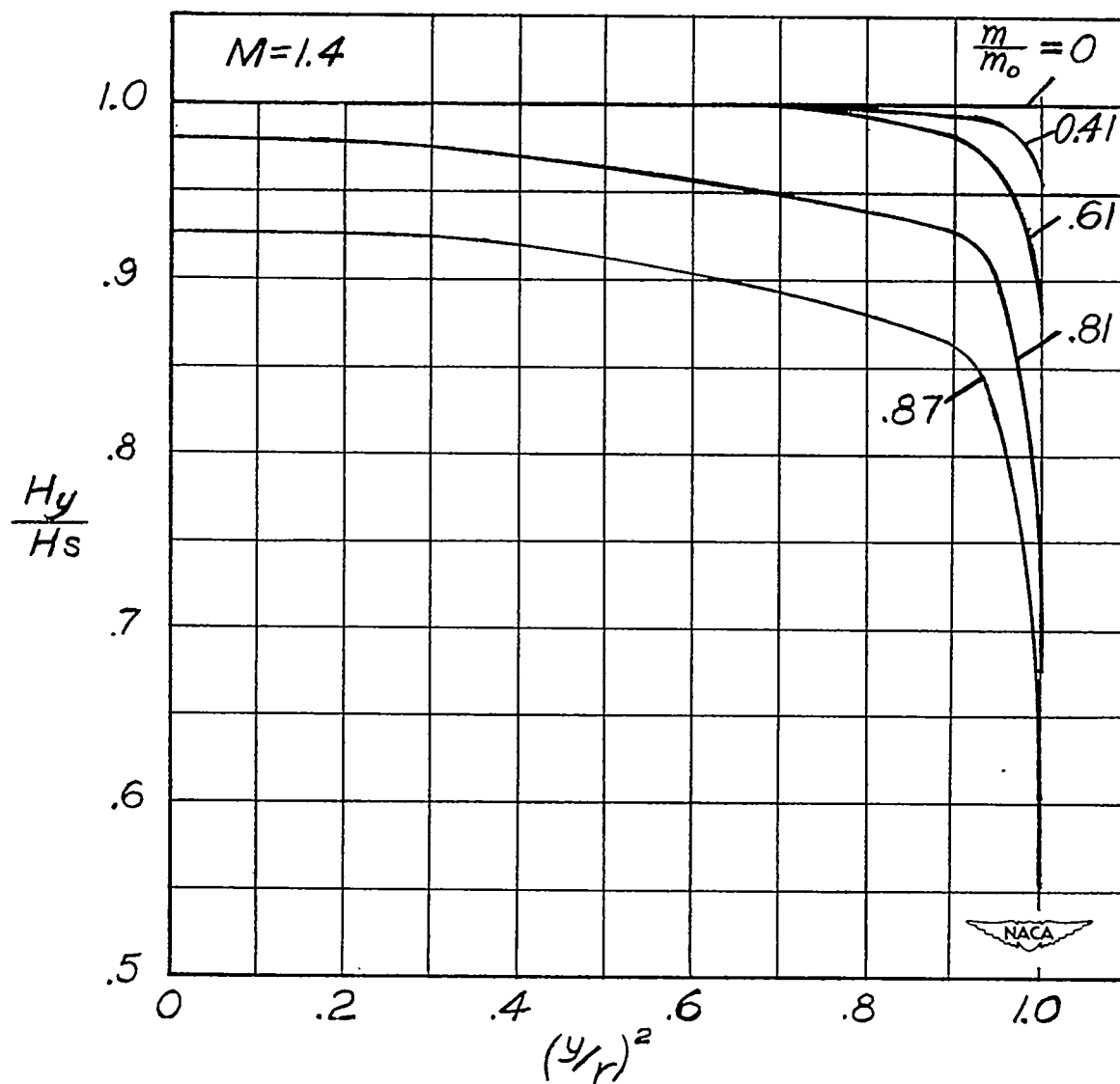Figure 9.- Measured external and computed additive drag coefficients
at a Mach number of 1.4.

Figure 10.- Total-pressure distributions at the throat station for various mass-flow ratios. Preflight-jet tests at M = 1.4.
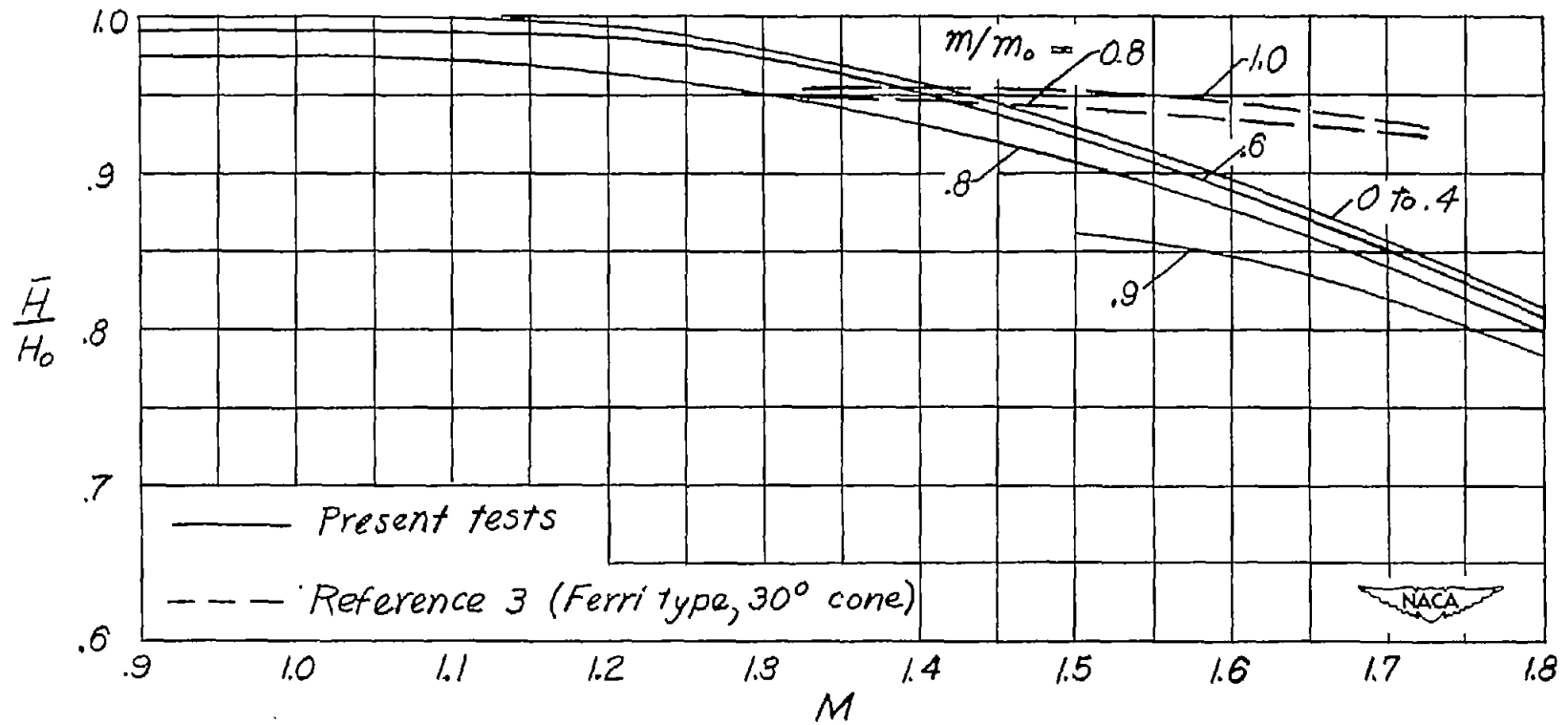
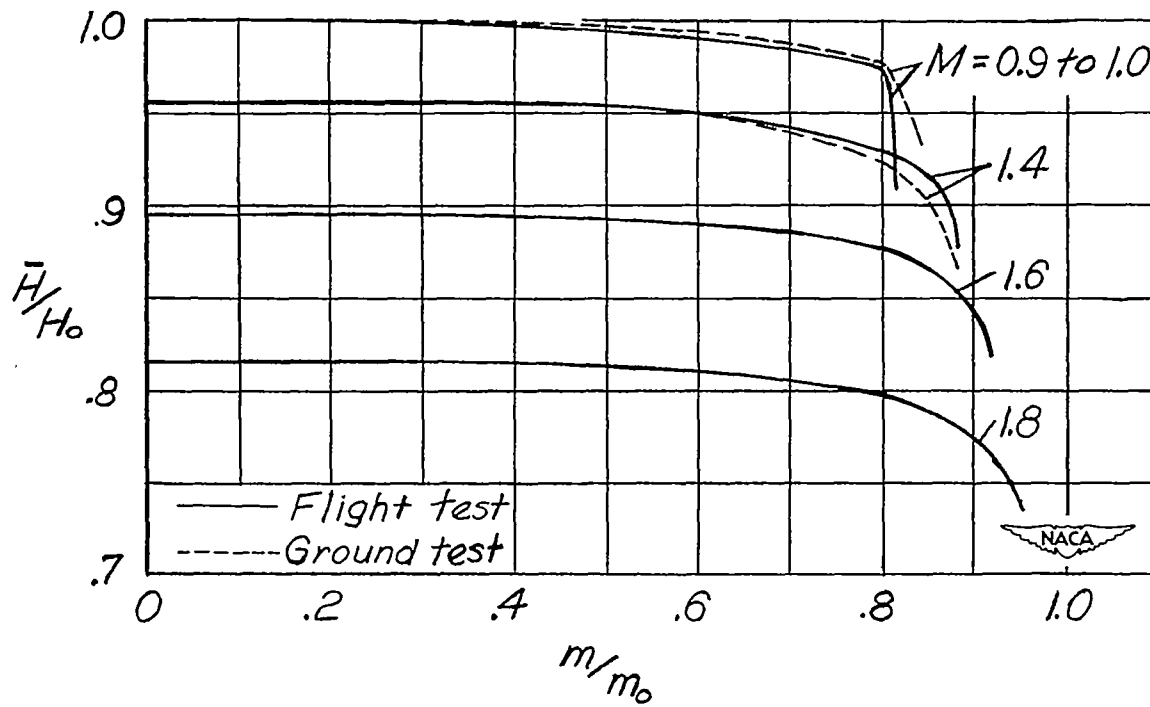Figure 11.- Variation of pressure recovery with Mach number for several mass-flow ratios.

Figure 12.- Variation of pressure recovery with mass-flow ratio for several Mach numbers.
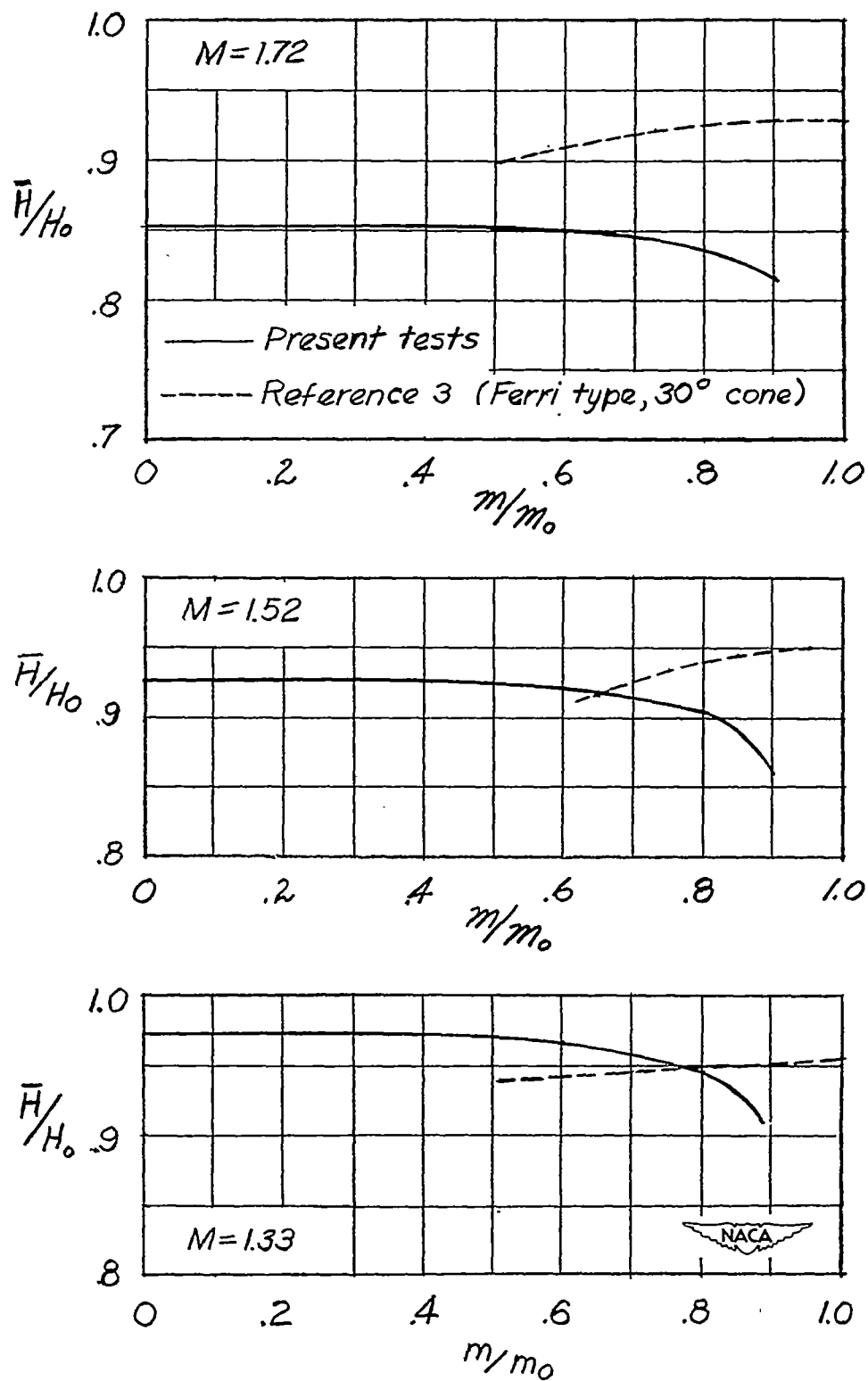
Figure 13.- Comparison of total-pressure recoveries from present tests
with those of a supersonic inlet of reference 3.